Sonoluminescing bubbles and mass diffusion

Ritva Löfstedt, Keith Weninger, Seth Putterman, and Bradley P. Barber
Department of Physics, University of California, Los Angeles, California 90024
(Received 29 November 1994)

The transduction of sound into light by a pulsating bubble in water occurs when its maximum radius is about ten times greater than its ambient radius. For such high-amplitude motion, the steady-state balance of mass flow between the bubble and gas dissolved in the surrounding fluid can be maintained by diffusion only at low partial pressures, about 3 Torr. The observation of sonoluminescence (SL) from bubbles in 200 Torr solutions of air in water requires the action of some as yet unknown mass flow mechanism. On the other hand, gas solutions prepared at low partial pressures, in the diffusion-controlled regime, enable one to achieve SL in gases that do not emit light at higher partial pressures. These include hydrogenic gases and gases with a ratio of specific heats close to unity, which hardly heat up upon adiabatic compression. Experiments that probe the role of mass transfer in SL are presented along with the implications of their comparison to a multiple-time-scale analysis of mass diffusion.

PACS number(s): 47.40.Nm, 78.60.Mq

Acoustic radiation pressure can trap a small gas bubble at the pressure antinode of a resonantly driven fluid [1]. For sufficiently high drive amplitudes the bubble pulsations can prevent its dissolution into the surrounding liquid [2,3]. At a threshold drive level, the oscillations of an air bubble in water become so nonlinear that the bubble collapses yield picosecond flashes of broadband light [4]. This light emission, sonoluminescence (SL) represents a concentration of the diffuse energy of the driving sound field by twelve orders of magnitude [5].

Light-scattering measurements have shown that this threshold to light emission is characterized by a bifurcation in the bubble dynamics (Fig. 1) [6]. The motion of the non-light-emitting, yet stably "bouncing" bubble is well described by the basic hydrodynamic equation. A small increase in the drive amplitude causes the bubble's ambient size (where the pressure of the gas inside it is the ambient pressure of 1 atm) to shrink, the expansion ratio of the maximum radius R_m to the ambient radius R_0 to grow sufficiently that the subsequent collapse becomes supersonic, and light to be emitted. A consideration of mass diffusion into and out of the oscillating bubble shows that, at a partial pressure of 150 Torr of air dissolved in the undersaturated water, the subthreshold bouncing bubble is a steady-state solution to the diffusion equation, while the SL bubble, where the acoustic radiative losses during the collapse suppress the after ringing, is not. Rather, for these experimental parameters, the stability of the light-emitting bubble implies the existence of a nondiffusive mass exchange mechanism. Conversely, calculating the conditions under which the SL bubble dynamics would be in diffusive equilibrium with the surrounding fluid has led to the observation of light emission in a new region of parameter space, characterized by extremely low partial pressures of dissolved gas (Fig. 2). In this diffusion-controlled regime of SL, we have succeeded in observing light emission from some gases that do not make the transition from bouncing to SL behavior at higher partial pressures.

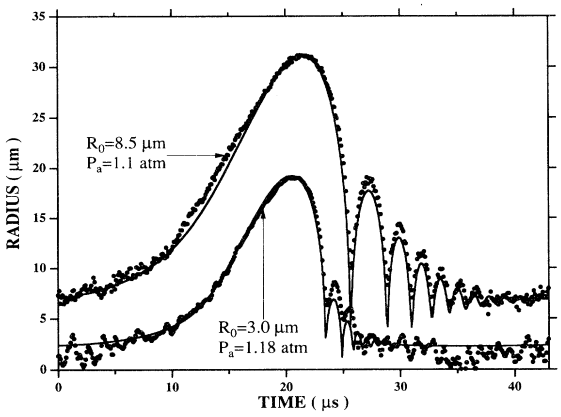

FIG. 1. Radius versus time for one cycle of the driving sound field for an argon-doped nitrogen bubble trapped in water. As the drive is increased the larger bubble abruptly shrinks, and the expansion ratio (R_m/R_0) increases. This bifurcation is due to a nondiffusive mass flow mechanism. Water is the only fluid in which we have succeeded in observing this transition. These measurements were carried at a partial pressure of gas of 150 Torr on a bubble that is 5% argon using the techniques of Ref. [3]. The solid line is a best fit to Eq. (1). The light-scattering technique is described in Ref. [27].

The observed sensitivity of SL to experimental parameters such as water temperature, sound level, and gas content of the bubble [6,7], suggests that stable SL in fluids other than water, which remains the only one in which it has been observed, could yield splendid surprises. Thus, en route toward the ultimate understanding of SL, the more immediate goal is to find the appropriate experimental conditions for light emission in these systems. The mass flow bifurcation of Fig. 1 characterizes a large region of SL parameter space, and may be a key to finding SL in other fluids and gases. Without resolving the question of the anomalous mass flow, we present the relevant phenomenology, theoretical and experimental, which will define the problem and so hopefully point to

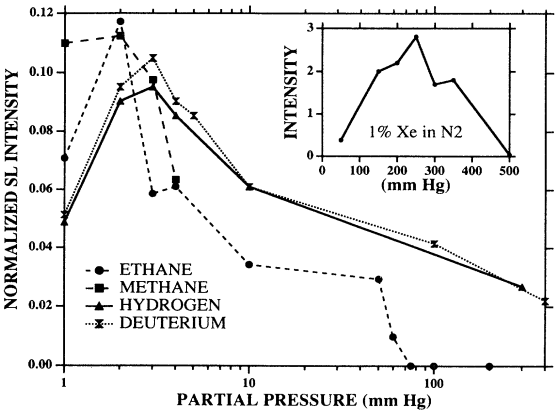

FIG. 2. Intensity of sonoluminescence, normalized to air of 150 mm and 20 °C, for various pure gases dissolved at low partial pressures. The inset shows the behavior of a nitrogen bubble doped with 1% xenon. Some gases, notably hydrogen and deuterium, are stable light emitters only at low partial pressures. The graph shows ethane intensities for bubbles, that last longer than 1 min. For ethane between 50 and 100 mm signals of about 0.03 could be seen for 5 to 25 sec. The experimental apparatus is discussed in Ref. [7].

its solution. The goal is an extension of the parameter space of SL as well as an interpretation of the second phase of single-bubble SL which occurs at partial pressures of a few Torr.

Theoretically, the diffusion equation closes the hydrodynamic description of the bubble motion by specifying the size of the bubble (i.e., the ambient radius) as a function of the experimental parameters. The Rayleigh-Plesset (RP) equation describes the motion of a bubble driven by a sound field [8–11],

$$R\ddot{R}+\tfrac{3}{2}\dot{R}^2=\frac{1}{\rho_l}\left[P_g(R)-P_0+P_a(t)+\frac{R}{c_l}\frac{d}{dt}[P_g(R)+P_a(t)]-\frac{2\sigma_l}{R}-\frac{4\eta_l\dot{R}}{R}\right]. \quad (1)$$

Here, the radius of the bubble $R(t)$ depends on the pressure of the gas inside it $P_g(R)$, the ambient pressure P_0, the drive pressure $P_a(t)$, and the density, speed of sound, surface tension, and viscosity of the fluid, ρ_l, c_l, σ_l, and η_l, respectively. The driven motion of the bubble is damped both by viscosity and by radiation of sound into the fluid. The RP equation is supplemented by an equation of state for the gas [10]. We choose this to be

$$P_g(R)=\frac{P_0R_0^{3\gamma}}{(R^3-a^3)^\gamma}, \quad (2)$$

where γ is the ratio of specific heats of the gas (and unity for an isothermal process), and R_0 is the ambient radius of the bubble, which is an undetermined parameter of the equation; "a" is the radius of the bubble's van der Waals hard core which arrests the violent collapse of the bubble ($a/R_0\approx 1/8.54$ for air). The nonlinear response of the driven bubble described by the RP equation displays the asymmetric motion that is the key to its energy-focusing properties (Fig. 3). When the driving pressure goes negative the bubble slowly and isothermally expands to its maximum radius. As the pressure turns to compression, the bubble collapses to its minimum size, where the light emission of an SL bubble occurs. In the shock wave model of SL [6,12], the energy of the bubble's adiabatic collapse is concentrated to even shorter length and time scales by the convergence of a spherical shock wave launched into the bubble interior as the bubble wall reaches speeds of order Mach 1. Following the collapse, the bubble oscillates as its natural frequency with diminishing amplitude until the next rarefaction phase of the drive. For the SL bubble, the energy of these oscillations is greatly diminished by the radiation of sound into the liquid during the supersonic collapse; the SL bubble remains virtually still at its ambient size for the second half of the acoustic cycle.

The differences between the bouncing and SL bubble motions for virtually the same drive parameters are attributable to their different ambient radii. Including diffusion determines the equilibrium size of the bubble by requiring no net mass flow across the bubble surface during a cycle. When the bubble is large and the gas pressure inside it is lower than the partial pressure to which

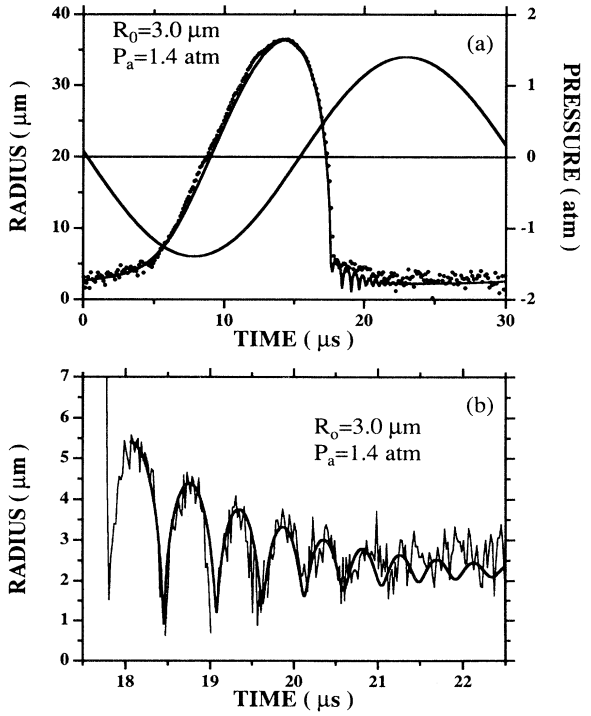

FIG. 3. Radius as a function of time for a light-emitting deuterium bubble at a partial pressure of 3 Torr. The driving sound field is shown along with (B) a detail of the after bounces. The solid lines are fits to the Rayleigh-Plesset equation (1).

the fluid is degassed, gas flows into it. When the bubble is small and the pressure inside it is high, gas flows out of the bubble into the surrounding fluid. For given drive parameters, the bubble for whose motion these two fluxes are equal is the steady-state solution.

Formally, the spherically symmetric diffusion equation for the concentration of gas in the fluid is

$$\frac{\partial C}{\partial t}+\frac{\dot{R}R^2}{r^2}\frac{\partial C}{\partial r}=D\nabla^2 C \ . \tag{3}$$

Here D is the diffusion coefficient ($=2\times10^{-5}$ cm^2/sec for air in water), and the convective term is determined by the velocity field of a pulsating bubble [10]. [Assuming that diffusion is a small effect on the size of the bubble, the RP equation (1), with the equation of state (2), determines $R(t)$ in (3); if diffusion is a large effect, the mass-conserving equation of state is no longer valid, and the diffusion and RP equations must be solved together (Appendix A).] The concentration of gas dissolved in the fluid at the bubble wall depends on the gas pressure inside the bubble according to Henry's law [13]:

$$C(r=R)=C_0 P_g(R)/P_0 \ , \tag{4}$$

where C_0 is the saturated concentration at 1 atm. Far from the bubble the concentration $C(r=\infty)=C_\infty$, which is determined by the extent to which the fluid is degassed. The rate of mass flux across the bubble wall is determined by

$$\left[\frac{dM}{dt}\right]_D=4\pi R^2 D\left[\frac{\partial C}{\partial r}\right]_{r=R} \ . \tag{5}$$

In the steady state the integral of the mass flux over one cycle of the motion must be zero. For the measured dynamics of a sub-SL bouncing bubble, the integral of the right-hand side vanishes, indicting that diffusion describes the mass transport for these steady-state bubbles. For the bubble dynamics of the SL regime of this same system, Eq. (5) implies that there is a net mass flow into the bubble each cycle and thus the bubble should increase in size with every cycle, or that there exists a supplementary nondiffusive mass flow mechanism.

The expression for the mass flow can be greatly simplified via a transformation to a moving reference frame that eliminates the convective term [3]. Defining

$$h=\tfrac{1}{3}(r^3-R^3) \quad \tau(t)=\int^t R^4(t')dt' \tag{6}$$

transforms the diffusion equation into the form

$$\frac{\partial C}{\partial \tau}-D\frac{\partial}{\partial h}\left[\left[1+\frac{3h}{R^3(\tau)}\right]^{4/3}\frac{\partial C}{\partial h}\right]=0 \ . \tag{7}$$

In the limit of a diffusive penetration depth small compared to the bubble radius, or

$$\delta_D=\sqrt{2D/\omega_a}\ll R_m \ , \tag{8}$$

the diffusion equation reduces to

$$\frac{\partial C}{\partial \tau}-D\frac{\partial^2 C}{\partial h^2}=0 \ . \tag{9}$$

The solution to (9) can be written

$$C(h,\tau)-C_\infty=A_0+\sum_{n=1}^{\infty}[A_n\cos(k_n h-\Omega_n\tau)+B_n\sin(k_n h-\Omega_n\tau)]e^{-k_n h} \ , \tag{10}$$

where

$$\Omega_n=\frac{2\pi n}{\tau(T_a)} \ , \quad k_n=\sqrt{\Omega_n/2D} \ , \tag{11}$$

and $T_a=2\pi/\omega_a$ is the acoustic period. In the steady state there can be no constant flow to infinity, so $A_0=0$, or

$$C_\infty=\frac{1}{\tau(T_a)}\int_0^{T_a}\frac{C_0 P_g(R)}{P_0}d\tau' =\frac{1}{\tau(T_a)}\int_0^{T_a}\frac{C_0 R_0^3}{R^3(\tau')}d\tau'=\langle C(0,\tau)\rangle \ . \tag{12}$$

Here we have used Boyle's law for the gas pressure $P_g(R)$ and the brackets denote a "time" average with respect to the variable τ. Boyle's law is an accurate description of the bubble dynamics during the slow expansion phase of the bubble as well as the inception of the collapse. It is not valid when the collapse reaches Mach 1, but the dilated time spent at these small radii is very short, and these terms do not contribute to the integral above.

Given the definition of τ the expression (12) is dominated by the time the bubble spends at its maximum radius and obeys the simple scaling relation, obtained by calculating (12) for the SL bubble dynamics;

$$\frac{C_\infty}{C_0}\approx 3\left[\frac{R_0}{R_m}\right]^3 \ . \tag{13}$$

For the sub-SL bouncing bubble (13) yields values of C_∞ that are consistent with the measured amount of gas dissolved in the fluid, for a variety of gases and concentrations (Fig. 4). Thus bubble dynamics can be used to determine the gas concentration in a fluid [10,14]. From the simple expression (13) it is clear that the threefold larger expansion ratio characterizing the light-emitting bubble would be in diffuse equilibrium with a much lower ambient concentration of dissolved gas. Assuming a typical SL expansion ratio of 10, which is the criterion for the bubble's runaway collapse to reach supersonic speeds as it passes through the ambient radius [6], the diffusion-limited regime of SL bubble dynamics should appear at partial pressures of a few Torr. By the same reasoning, this region of SL parameter space should not admit a steady-state bouncing bubble since such a bubble would dissolve into the degassed fluid. The low partial pressure regime of stable SL has been observed for a variety of gases, including certain polyatomic ones, characterized by a γ very close to unity, which do not give light at higher partial pressures (Fig. 2). These observations suggest that the SL light-emission mechanism is effective even without adiabatic heating. The pure noble gases,

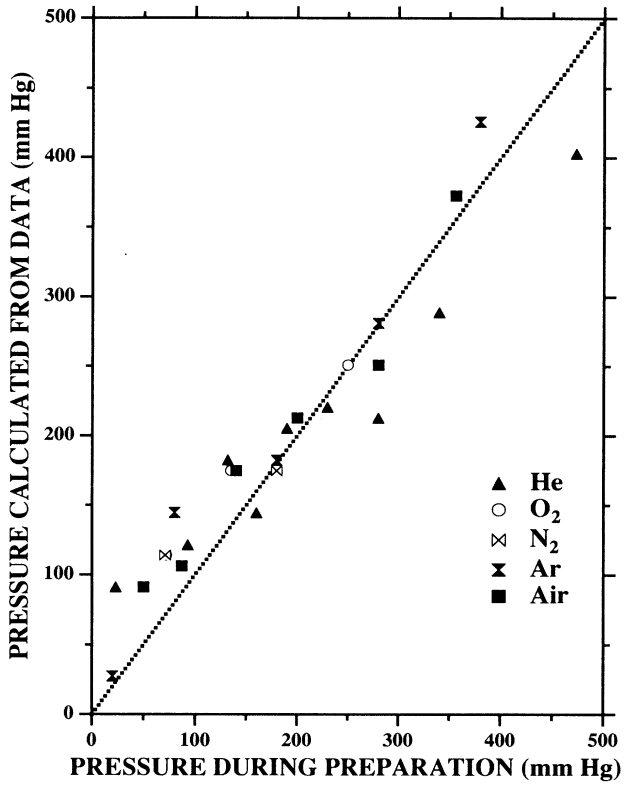

FIG. 4. Static versus diffusive partial pressures. The abscissa shows the pressure at which gas has been stirred into the water, and the ordinate shows the pressure calculated from the application of the diffusion equation to the measured low-amplitude, steady-state bubble motion.

which emit the same light intensity throughout the range of partial pressures, are more stable at the lower partial pressures. The noble-gas-doped nitrogen bubbles that are the brightest at the higher partial pressures [7] do not show any peak in intensity at the diffusion-limited parameters. No SL has been seen from pure nitrogen bubbles at the low pressures where they are completely unstable.

The data showing the abrupt transition between a bouncing bubble and a light-emitting bubble was taken at a partial pressure of air in water of 150 Torr (which is about the amount of air that dissolves into degassed water when it is poured from one flask to another under normal room conditions). Given the light-scattering measurements of the bubble dynamics in this SL regime, one can calculate the amount of mass that flows into the bubble from infinity each cycle. Since the bubble is in a steady state this same amount of mass must somehow be nondiffusively ejected again. The diffusion process described by Eq. (7) is characterized by two separate time scales. The bubble motion defines the short time scale, during which the mass flow is restricted to a diffusive penetration depth around the bubble. On the longer time scale, mass can flow steadily from the bubble wall to infinity. Thus we can define the concentration of gas in the fluid as

$$C(h,\tau)=\bar{C}(h,\bar{\tau})+\sum_n C_n(h,\bar{\tau})\cos(n\Omega_a\tau+\delta_n)\ , \tag{14}$$

where $\bar{\tau}$ is the long time scale that changes only a small amount during a cycle. In this equation, $\bar{C}(h,\bar{\tau})$ is a slowly varying function of time and space, and $C_n(h,\bar{\tau})$ drops off exponentially for distances beyond a penetration depth. Averaging Eq. (7) over one acoustic period gives

$$\frac{\partial\bar{C}}{\partial\tau}-D\frac{\partial}{\partial h}\left\langle\left[1+\frac{3h}{R^3(\tau)}\right]^{4/3}\frac{\partial C}{\partial h}\right\rangle=0\ , \tag{15}$$

where angular brackets indicate an average over one cycle. In the steady state $\bar{C}(h,\bar{\tau})$ is independent of τ, and in the far field of the bubble where $h\gg\delta_D R_m^2$ and the coefficients of the oscillatory terms $C_n(h,\bar{\tau})$ are zero, (15) yields

$$\frac{\partial\bar{C}}{\partial h}\approx\frac{B_0/R_m^3}{\left\langle\left[1+\frac{3h}{R^3(\tau)}\right]^{4/3}\right\rangle}\ . \tag{16}$$

Noting that the time average in the denominator of (16) is dominated by the maximum radius, and integrating the right-hand side with respect to h yields

$$\bar{C}(h,\bar{\tau})\approx\frac{B_0(\bar{\tau})}{\left[1+\frac{3h}{R_m^3(\bar{\tau})}\right]^{1/3}}+C_\infty\ , \tag{17}$$

where we note that $R_m^3(\bar{\tau})$ can be changing on the long time scale $\bar{\tau}$. The factor B_0, which is a constant on the short time scale, is fixed by matching (17) to the near-field solution, i.e., for $\delta_D R_m^2\ll h\ll R_m^3$, where Henry's law determines the concentration since $\bar{C}(h,\bar{\tau})$ is a slowly varying function of h. The resultant expression is [2],

$$\bar{C}(h,\bar{\tau})\approx\frac{\bar{C}(0,\bar{\tau})-C_\infty}{\left[1+\frac{3h}{R_m^3(\bar{\tau})}\right]^{1/3}}+C_\infty\ . \tag{18}$$

Since, for the case under consideration, $C_\infty\gg\bar{C}(0,\bar{\tau})$, the mass influx to the bubble per cycle, evaluated by using (18) in Eq. (5), is $\Delta M\approx 2\pi DC_\infty R_m T_a$. The fraction of mass in the bubble that must be ejected per cycle in order to maintain the steady state is, therefore, given by

$$\frac{\Delta M}{M}\approx\frac{3}{2}\left[\frac{T_a D}{R_0^2}\right]\frac{C_\infty}{C_0}\frac{C_0}{\rho_0}\frac{R_m}{R_0}\approx 10^{-4}\ , \tag{19}$$

where ρ_0 is the ambient density of the gas (for air, ρ_0 is 1.02×10^{-3} g cm^3 and $C_0/\rho_0\approx 0.02$). This is a very small portion of the collapsed bubble, but the process that leads to this ejection is the key to SL in a single bubble.

A candidate source of this mass ejection is the extremely high pressure P_c characterizing the bubble at its minimum radius R_c. Although the applicability of the sample hydrodynamic model to the bubble's collapse is questionable, the solution of the RP equation (1) and the equation of state (2) gives a maximum pressure P_c of 10^5

atm, lasting for a time $\Delta t_c \approx 10$ psec [10]. Extrapolating Henry's law to this extreme implies that for an air bubble in water the maximum concentration C_c of air dissolved in the water near the minimum radius is twice the density of water. A more reasonable ansatz would set the maximum fraction of air molecules in the water to be one in ten. Using this ansatz in (5) and choosing the diffusive penetration depth appropriate to Δt_c as the length scale of the concentration gradient gives for the mass ejected at the minimum

$$\Delta M_c \approx 4\pi a^2 C_c \sqrt{D \Delta t_c} \ . \tag{20}$$

This quantity is approximately that required by (19) to compensate for the diffusive mass influx. However, this outburst of mass at the bubble's minimum does not lead to a net flow to infinity. Instead, using the assumed value for C_c in evaluating Eq. (12) shows that the contribution of the collapse to the determined of C_∞ is down by the factor $\Delta t_c / T_a$ from the mass influx during the bubble expansion. The parabolic nature of the diffusion equation is such that during the short duration of the collapse the ejected mass hardly penetrates the liquid. Rather than feeling the boundary condition at infinity, the concentration instead follows Henry's law, and flows back into the bubble during the rest of the cycle. The bubble's spherical geometry amplifies this effect, since mass conservation, in the absence of mass exchange across the bubble surface, implies that the surface layer of dissolved gas near the bubble becomes thinner as the bubble grows, steepening the concentration gradient and increasing the mass inflow. The net effect of this process is contained in Eq. (12). Thus the anomalous mass flow of (19) must be a nondiffusive mechanism, and the ejected mass must be displaced beyond the penetration depth of the bubble motion. In the shock wave model of SL the ejection could perhaps be associated with the imploding shock launched by the collapsing bubble which collides with the bubble wall after reflecting off the origin. Assuming that the mass is ejected at the minimum radius of the bubble, where the diffusion equation is most likely to be violated, the mass fraction (19) corresponds to a shell of compressed gas which is less than 1 Å thick. This small mass ejection underlies the transition to SL.

Within a single cycle of the motion the diffusion process leads to fluxes that are generally larger than (19). These fluxes can be approximated by assuming that mass flows out of the bubble during that half of the cycle when its radius is virtually still at R_0. Approximating the gradient in concentration by using the diffusive penetration depth, δ_D, as a characteristic length scale, the change in the mass of the bubble during half of a cycle due to diffusion is

$$\left[\frac{\Delta M}{M}\right]_D \approx D \frac{C_0}{\delta_D} \frac{T_a}{2} \frac{1}{\rho_0 R_0} \approx \frac{\sqrt{\pi}}{2} \frac{C_0}{\rho_0} \frac{\sqrt{D T_a}}{R_0} \approx 10^{-2} \tag{21}$$

which agrees with a more careful analysis based on integrating (10) over a half a cycle. Note that the oscillatory contribution to mass transfer (21) is independent of C_∞, as follows from evaluating the coefficients A_n and B_n (for $n \neq 0$) in (10) subject to the boundary condition (4). This flow is sufficiently small that the basic formulation of the bubble dynamics (1) is not affected. However, the numbers given above apply only for air in water. For air in other liquids the factor C_0/ρ_0 is larger by a factor of 100 or more. In fact, perhaps the anomalously low solubility of gases in water [15] facilitates the occurrence of SL. In other fluids, such as silicon oil, the mass flux during the expansion part of the cycle can equal the original mass in the bubble and significantly alter the bubble dynamics. In particular, the collapse of the bubble may be weakened by the extra cushion of gas absorbed during the expansion. Perhaps this explains why at high partial pressure a gas bubble in silicon oil can display bouncing motion, but does not make the transition to a supersonic collapse (Fig. 5). Substantial mass transfer across the bubble surface may also shift the phase of the bubble motion with respect to the acoustic drive, affecting the trapping of the bubble at the pressure antinode (Appendix B). This analysis suggests a possible route to finding the parameter space of SL in other fluids. Combining other fluids with low solubility gases such as helium and hydrogen will lower the C_0/ρ_0 to the air-water level.

The apparent mystery of the occurrence of SL at the higher partial pressures where diffusion is disobeyed is added to by further investigation. The abrupt transition to SL characteristic of air and noble-gas-doped nitrogen contrasts with the same measurement of the phase space of pure argon bubbles. There the transition to SL is continuous, and the discrepancy between diffusion and the bubble dynamics increases smoothly with the drive level and the light intensity [7]. A pure nitrogen bubble whose SL intensity is only 1/30th that of air is rather unstable

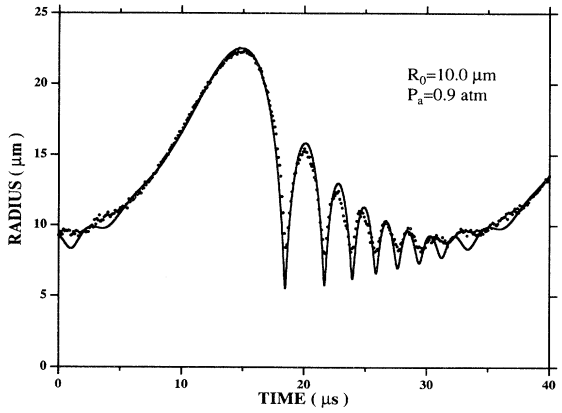

FIG. 5. Radius versus time measurements of a helium bubble trapped in low viscosity silicon oil. This non-light-emitting bubble is driven at 30.9 kHz. [The speed of sound in this silicon oil is 954 m/s, the specific gravity is 0.91, and the shear viscosity is 1 centistoke ($=10^{-2}$ cm^2/s).] The helium was mixed at a partial pressure of 165 mm. At higher drive levels, a mass flow bifurcation, like that of Fig. 1, cannot be seen, and the expansion ratios characteristic of SL have not been achieved in this system. The solid line is a best fit to Eq. (1).

and jittery, while a bouncing nitrogen bubble is stable. Despite the different behaviors of these gases, however, the "anomalous" mass flow process is a characteristic of each, since the law of partial pressures requires the thermodynamic equilibrium of the gaseous phase and the dissolved gas to apply to each component separately. The generalization of (13) to a mixture of gases is

$$\frac{P_{\infty,i}}{P_0}=\frac{C_{\infty,i}}{C_{0,i}}\approx 3\left[\frac{R_0^3}{R_m^3}\right]\frac{P_{\infty,i}}{\sum_i P_{\infty,i}} . \tag{22}$$

Using the expansion ratio typical of SL bubble dynamics to compare the first and third term in (22) shows that given a mixture of gases, which experimentally has been shown to give light at high partial pressures, each gaseous component will likely violate diffusion. [There are values of the parameters for which (22) is satisfied, but such isolated, coincidental solutions do not suffice to describe the richness of the SL parameter space.] While some rectification process that concentrates one of the gases in the bubble may exist, implying that Henry's law is violated, the underlying dynamics must involve each gas dissolved in the liquid.

As mentioned already by Rayleigh [8], the equation describing the violent collapse of the bubble also predicts huge pressure gradients in the fluid right near the interface. Associated with such gradients is an additional term in the diffusion equation

$$\frac{\partial C}{\partial \tau}-D\frac{\partial}{\partial h}\left[\left[1+\frac{3h}{R^3(\tau)}\right]^{4/3}\left[\frac{\partial C}{\partial h}+\frac{k_P}{P}\frac{\partial P}{\partial h}\right]\right]=0 , \tag{23}$$

where k_P is the barodiffusion coefficient [16]. In the limit of a dilute concentration of gas in the liquid [17],

$$\frac{k_P}{P}\approx\frac{C}{\rho_l c_0^2} , \tag{24}$$

where c_0 is the ambient speed of sound in the gas (3.4×10^4 cm/sec for air). Since the pressure gradients are largest when the bubble is at its minimum size, we estimate the effect of the pressure term by comparing the two contributions to the mass flux at the minimum,

$$\frac{\Delta M_P}{\Delta M_c}=\frac{\frac{k_P}{P}\frac{\partial P}{\partial h}}{\frac{\partial C}{\partial h}}\approx\frac{P_c}{\rho_l c_0^2}\frac{\sqrt{D\Delta t_c}}{a} . \tag{25}$$

Here the length scale characterizing the pressure gradient in the fluid is the minimum bubble radius,which is limited by the van der Waals hard core. The ratio in (25) is of order unity, and the earlier comments regarding the mass ejected at the minimum by an extrapolation of Henry's law apply to barodiffusion as well. To evaluate the effect of barodiffusion, we model it as a δ-function shell of mass ΔM_P outside the bubble, at $r\approx 2a$. Solving the diffusion equation (9), subject to this initial condition, and the boundary condition that the concentration at the bubble is held fixed at $C(h=0,\tau)=0$, gives [18]

$$C(h,\tau)\approx\frac{\Delta M_p}{2\sqrt{\pi D\tau}}\left[\exp\left\{\frac{-(h-2a^3)^2}{4D\tau}\right\}-\exp\left\{\frac{-(h+2a^3)^2}{4D\tau}\right\}\right] . \tag{26}$$

Integrating the expression (26) over all h gives the net mass in the fluid due to the barodiffusive ejection. Initially, this mass is simply ΔM_P. For long times this integral is

$$\lim_{\tau\gg a^6/D} M_P(\tau)\approx\Delta M_P\frac{2a^3}{\sqrt{\pi D\tau}} . \tag{27}$$

After one acoustic cycle, only one part in 10^4 of the ejected mass is still in the fluid. Because the hard-core radius "a" is of the same order as δ_D, the mass outflow due to the pressure gradient at the collapse simply diffuses back into the bubble during the rest of the acoustic cycle.

The preceding analysis of mass transport also neglects effects of acoustic streaming, which by its nature extends over distances large compared to δ_D. Previous experiments with one millimeter bubbles have suggested that quadrupolar shape oscillations of a bubble enhance mass transport across its surface [19]. Evidence for the spherical symmetry breaking associated with the streaming velocities has not yet been observed in the SL bubble motion. Analysis of the corrugation (Rayleigh-Taylor) instabilities associated with the accelerating wall of the bubble [20–22] suggests that the sphericity of the bubble is maintained in the course of its nonlinear oscillations (Appendix C). The dynamics typical of the SL bubble, which spends one half of each acoustic cycle motionless at its ambient radius, contrasts with the long time scales required for the establishment of mass convection cells. For example, a quadrupolar perturbation of the bubble shape decays with a time constant of less than 1 μsec while the bubble is motionless at its ambient radius for more than 10 μsec. Rather than the bubble dynamics slaving to a preexisting flow field, it appears that the bubble begins each cycle without any memory of its previous motion.

Any theoretical approach to understanding SL must grapple with the broad range of time scales characterizing the phenomenon. Dynamically, diffusion is a very slow process. Applying the diffusion equation to a quiescent bubble, where the convective term can be neglected, gives the time for a bubble to dissolve into a degassed liquid [23],

$$t_D\approx\frac{1}{2}\frac{\rho_0 R_0^2}{D(C_0-C_\infty)} . \tag{28}$$

According to (28) a 5-μm air bubble will dissolve in degassed water in a fraction of a second. Alternatively, given a typical drive frequency of 40 kHz, the time for a driven bubble to grow to its ambient size from an infinitesimal radius according to Eq. (19) is also on the order of a second. If the sound amplitude driving a weakly light-emitting bubble is suddenly increased, the bubble

will grow to a new equilibrium size and simultaneously increase the intensity of its emission on precisely this time scale. The SL of doped-nitrogen bubbles can display oscillations in the light intensity [7]; these are accompanied by oscillations in the radius of the light-emitting bubble, with the same period of seconds (Fig. 6). While a solution of the coupled equations of diffusion and bubble motion would describe a smooth approach to the steady state (Appendix A), these oscillations represent an "overshoot" of the mass flow mechanism, absent from such a description. Rather, one could wonder whether the inertia associated with these oscillations is a characteristic of the anomalous mass flow mechanism.

Experimentally, the dynamic mass range processes can also be probed by measuring the turn-on time of driven bubbles (Fig. 7). A bubble is seeded into the isolated resonator by means of a toaster wire, which, when heated, boils the liquid and creates a vaporous cavity [7,14]. Before this can collapse, dissolved gas from the fluid flows into it, and it is subsequently trapped by the sound field. The time that elapses between the seeding of the bubble and the subsequent light emission shows surprising variability as a function of the gas dissolved in the fluid and of the drive amplitude. The noble gases, when driven at a low amplitude, reach their maximum brightness within fractions of a second of being seeded. The same behavior characterizes higher drive levels, where the eventual light emission is ten times brighter. These bubbles can be seen to emit light as they rise from the nichrome wire on the way to the pressure antinode of the sound field. A noble-gas-doped nitrogen (or air) bubble turns on slowly. At low drive levels, it emits little or no light for some seconds before abruptly climbing to its steady SL value. When driven harder, it first attains a low level of light emission, comparable in intensity to the more weakly driven one. After a second or so of very slow and irregular increases in light intensity, the bubble brightness then exponentially approaches its steady state, smoothly increasing in brightness by a factor of 10 on time scales of about 5 sec. These behaviors characterize the turn ons at both low and high partial pressures of dissolved gas. It is unclear whether the doped bubble's slow approach to its enhanced brightness is the result of some mass exchange process or a signature of the light-emitting mechanism itself.

An effect of surface tension on the transition of SL is shown in Fig. 8 which displays the radius-versus-time cues of a 1% xenon in nitrogen bubble at 150 Torr for increasing drive levels. Above the bouncing regime, there occurs a mass flow bifurcation similar to that in Fig. 1. At this point the bubble shrinks, and the expansion ratio increases as shown in Fig. 9. But as the sound field is increased further the transition to SL is hindered by the action of surface tension on the small bubble. For these bubbles $2\sigma_l/R(0)$ is comparable to $P_a(0)-P_0$, where time is now measured from the moment of maximum

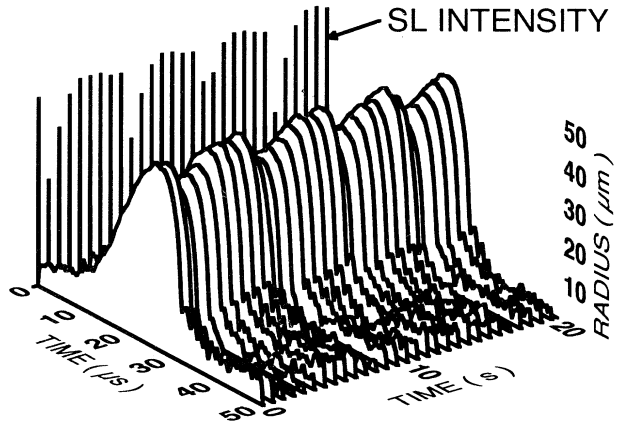

FIG. 6. SL intensity and bubble radius as a function of time for a nitrogen bubble with 5% argon. At a drive level just below the upper threshold of SL this bubble shows a variation on a long time scale of the order of 4 sec. The acoustic frequency is 23 kHz, and the gas is dissolved at 150 Torr.

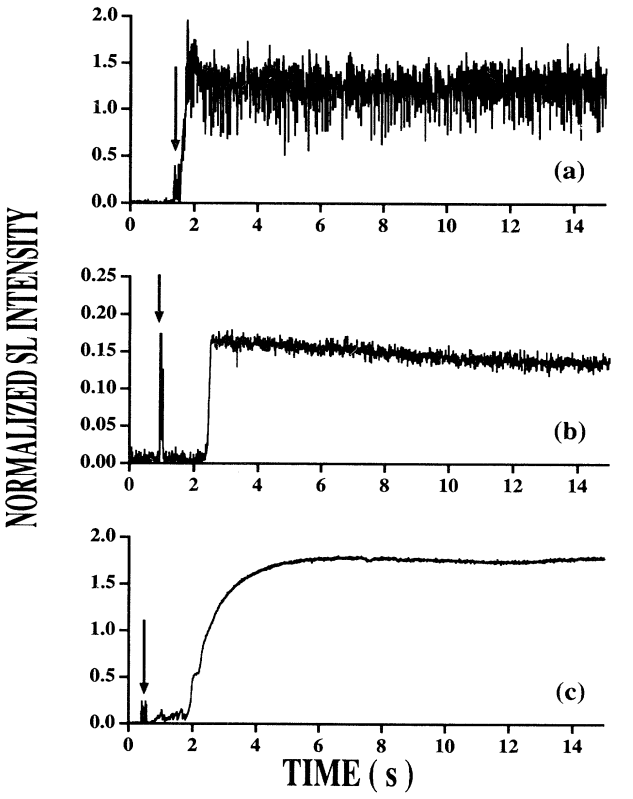

FIG. 7. Turn-on times for SL. Shown is the light intensity as a function of time after seeding a bubble into an acoustically driven resonator. In (a) a pure xenon bubble at high drive levels lights up almost instantaneously. In fact, these bubbles are glowing as they leave the toaster wire on their way to the velocity node of the sound field. (b) and (c) show the response of a xenon-doped nitrogen bubble. An arrow indicates a flash of light from an LED that is activated by the current through the nichrome wire. This is the moment of seeding the gas bubble. Note the plethora of time scales that characterize the bubble driven at a high amplitude (c). These experiments were carried out in a cylindrical plexiglass resonator.

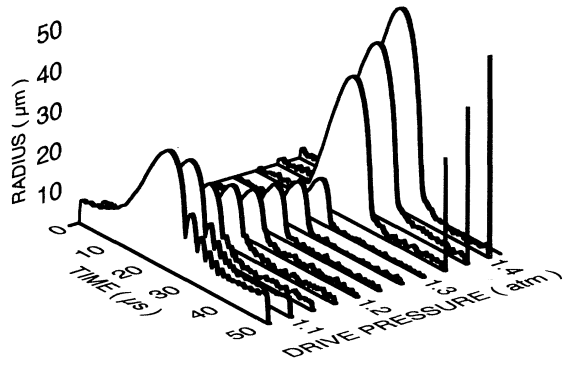

FIG. 8. Radius versus time for a 1% xenon-doped nitrogen bubble as a function of increasing drive level. The relative intensity of SL is indicated by the vertical lines. The transition to SL occurs only after the force of surface tension on the small bubbles is overcome by the driving sound level. The partial pressure is 150 Torr.

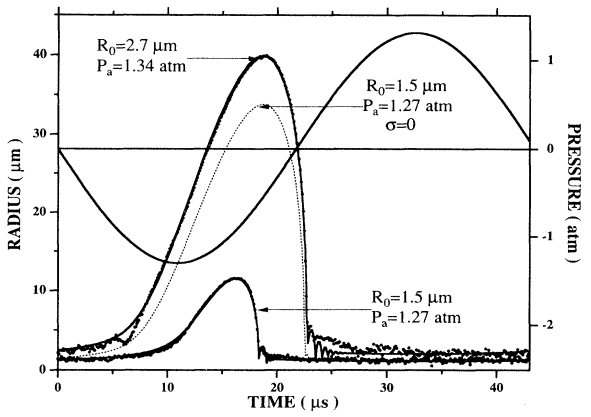

FIG. 10. Detail of the radius versus time showing the transition from a small bubble to an SL bubble. This transition is dominated by the effect of surface tension as can be seen from the plot (dashed line) of the solution to Eq. (1), where σ_l has been set equal to zero. (For the solid line fits, we have used $\sigma = 50$ dynes/cm.)

rarefaction of the drive. Since the rate of expansion scales as

$$\dot{R} \approx \left[\frac{P_a(0) - P_0 - 2\sigma_l / R(0)}{\rho_l} \right]^{1/2}, \tag{29}$$

the action of surface tension on a small bubble can inhibit the realization of a large R_m as shown in Fig. 10. When the drive level exceeds the dynamic thresholds determined by surface tension and P_0, the increase in bubble radius can be dramatic since the elastic force decreases further as the radius increases.

When surface tension is important the bubble motion can display hysteresis. For example the transition to SL for a 0.1% xenon in nitrogen bubble at 150 Torr is shown in Fig. 11. Note that SL is separated from the non-light-emitting regime by a region where there is no steady-state bubble motion. Within the non-SL region, an upward sweep in drive amplitude marches from bubble to bubble regardless of the rate of increase of the acoustic pressure.

However, an infinite step to lower P_n will cause the bubble to disappear. Nor can such a bubble be reseeded at the drive level at which it disappeared; to recover the stable small bubble, one must start with a lower-amplitude bouncing bubble and increase the drive level.

For pure noble gases the transition to SL can be smooth [7] rather than displaying the abrupt bifurcation of the air bubble. The transition of a 5% noble-gas-doped nitrogen bubble lies between the limiting behaviors of 1% and pure bubbles (Fig. 12). In cases like this, the higher-amplitude bouncing bubble parameters already show some deviation from diffusion theory.

The hydrodynamic theory of SL, even as supplemented by diffusion, is necessarily incomplete, as it lacks any light-emitting mechanism. Phenomenologically, SL is characterized by complementary traits: its remarkable sensitivity to small changes in experimental variables and

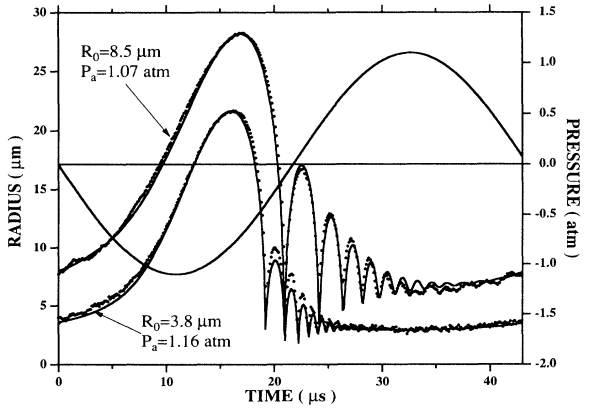

FIG. 9. Detail of the radius versus time for a 1% xenon-doped nitrogen bubble at the mass flow bifurcation.

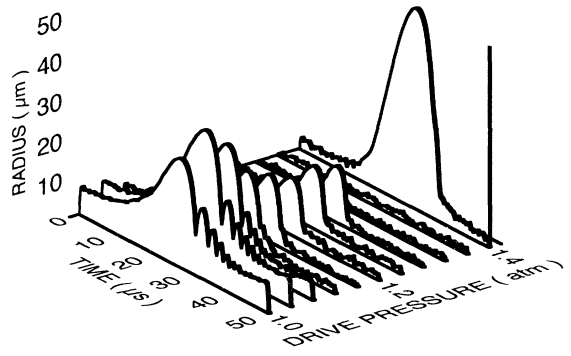

FIG. 11. Transition to SL for a 0.1% xenon bubble at 150 mm. These radius versus time curves were taken as a function of increasing drive level. As the drive is decreased, the small bubbles cannot be reseeded. Those states must be approached from the lower-amplitude, bouncing-bubble regime.

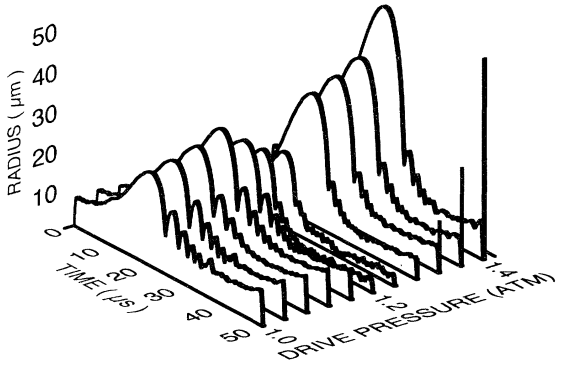

FIG. 12. The transition to SL for a 5% argon in nitrogen solution at 150 mm. Figure 1 is a detail from this waterfall plot.

the robustness of its steady state [24]. These two properties guide the hydrodynamic theory. The robust nature of the phenomenon in the systems in which it has been seen, suggests that the underlying mechanism of the energy concentration is generalizable to other regions of the vast phase space. The startling sensitivity of SL to controllable variables urges one to uncover the properties of the light emission, and the limits of the energy focusing, in these other systems. As for diffusion, the discovery of a new window in phase space is accompanied by more questions for the theorist. Indeed the measurements indicating the anomalous mass flow and the dependence of the light intensity of air bubbles on their one percent argon component, make the original SL discovery [25] seem all the more "fortuitous" [26]. Surely even more discoveries lie in wait as the parameter space of SL is expanded and explored.

We are obliged to P. H. Roberts for valuable comments and key help with the derivation of expression (18), and to L. P. Pitaevskii for helpful discussions. We are indebted to R. Hiller for valuable advice and ideas. We are grateful to A. Prosperetti for bringing Ref. [2] to our attention. This research is funded by the USDOE Office of Basic Energy Science, Division of Advanced Energy Projects (experiment) and Division of Engineering and Geophysics (theory).

APPENDIX A: COUPLING THE RAYLEIGH-PLESSET AND THE DIFFUSION EQUATIONS

If diffusive mass flow significantly affects the number of gas molecules in the bubble, the mass-conserving equation of state (2) no longer applies. Instead, the self-consistent solution of the RP equation (1) and the diffusion equation (3) determines the radius of the bubble $R(t)$ and the number of gas molecules in the bubble, $N_g(t)$. In terms of these quantities (and neglecting heat flow into the bubble, which is studied in detail by Prosperetti [11]), the generalized equation of state is

$$P_g(R,N_g)=\frac{P_0(\mathcal{R}T_0/P_0)^\gamma}{(R^3/N_g-b^3)^\gamma}\ , \tag{A1}$$

where T_0 is the ambient temperature of the fluid, $\mathcal{R}$ is the ideal gas constant, and P_0 is the ambient pressure. The excluded volume of a gas molecule is $4\pi b^3/3$.

The diffusion of gas from the bubble wall into the fluid determines the change in the number of gas molecules in the bubble. This change is given by (5), which in the transformed variables is

$$\left[\frac{dN_g}{d\tau}\right]_D=\frac{4\pi D}{\mathcal{M}}\left[\frac{\partial C}{\partial h}\right]_{h=0}\ , \tag{A2}$$

where $\mathcal{M}$ is the molecular weight of the gas. The concentration gradient of the gas at the bubble can be determined by a solution to the diffusion equation (3). The concentration at the surface is fixed by Henry's law (4), where the pressure in the gas is a function of both the bubble radius and the number of gas molecules in the bubble according to (A1). The coupling of hydrodynamics to diffusion entails simultaneous solution of the RP equation (1) with the equation of state (A1), and the diffusion equation (3) and (A2). It remains to be seen whether this coupling affects the phasing of the $R(t)$ curves relative to the sound field.

APPENDIX B: TRAPPING AN SL BUBBLE

In SL the effectiveness of the sound field is dramatic. The drive oscillations of the bubble are the initial stage of the energy focusing which eventually leads to the light emission. Coupled with diffusion, the bubble pulsations prevent it from dissolving in the degassed fluid. More fundamentally, the sound field stabilizes the bubble against the force of buoyancy, and traps it at precisely the location where its effect on the bubble is the greatest. The time-averaged force on a bubble in a standing-wave sound field is [1]

$$\vec{F}_a=-\langle V\vec{\nabla}P_a\rangle\ , \tag{B1}$$

where V is the bubble volume. For small oscillations the acoustic radiation (or Bjerknes) forces are a second-order effect in the drive amplitude. For an SL bubble, the time-averaged force is dominated by the expansion of the bubble, when the volume is the largest and the drive pressure passes through an ascending node (Fig. 3). Approximating the time-averaged radius as one half of its maximum value and the duration of the expansion as one fourth of the acoustic period gives for the radiation force

$$F_a=\frac{1}{4}\frac{4\pi}{3}\left[\frac{R_m}{2}\right]^3 P_a' k_z^2 z\ , \tag{B2}$$

where P_a' and k_z are the amplitude and the wave number of the $\hat{z}$ component of the sound field, and "z" is the distance of the bubble from the pressure antinode. This net force is directed toward the pressure antinode of the sound field. Note that because of the great asymmetry in the SL bubble motion, the radiation force is linear in the driving pressure.

As in the force (B2), the effect of buoyancy is greatest when the volume of the bubble is a maximum. To find the equilibrium location of the bubble, one balances (B2) with the buoyant force

$$F_b=\rho_l g\langle V\rangle\approx\frac{1}{4}\frac{4\pi}{3}R_m^3\rho_l g\ . \tag{B3}$$

Here, gravity acts in the $\hat{z}$ direction. For a typical acoustic drive frequency of 25 kHz and a dynamic amplitude of one atmosphere, the distance of the bubble from the antinode,

$$\langle z\rangle=\frac{8\rho_l g}{P_a' k_z^2}\ , \tag{B4}$$

is less than a millimeter. In addition one can estimate the movement of the bubble about this equilibrium position as during its radial oscillations. Here the radiation force acts on the effective mass of the bubble,

$$\frac{2\pi}{3}R^3\rho_l\ddot{z}(t)=F_a(t)+F_b(t)$$
$$\approx\frac{4\pi}{3}R^3P_a'\sin(\omega_a t)k_z^2 z(t)-\rho_l g\frac{4\pi}{3}R^3\ . \tag{B5}$$

Because the coefficient of the time-dependent pressure term is small compared to the inertia of the displaced fluid, the solution to (B5) can be written as

$$z(t)\approx\langle z\rangle+\langle z\rangle\left[\frac{P_a'}{2\pi\rho_l c_l^2}\right]\sin(\omega_a t)\ , \tag{B6}$$

and the excursions of the bubble from its equilibrium position are seen to be negligible.

APPENDIX C: THE RAYLEIGH-TAYLOR INSTABILITY

A plane interface between two media of different densities is unstable to corrugation if the lighter one is accelerated towards the heavier one (or, in a gravitational field, if the heavy one is on top). For a gas bubble in a liquid, the exponential growth of the angular surface perturbations, which characterizes the planar Rayleigh-Taylor instability [20], is accompanied by effects related to the spherical geometry [21,22]. Following these references, we write the radius of the bubble as

$$R(t)=\bar{R}(t)+\sum_{n=2}^{\infty}a_n(t)Y_n(\Theta,\Phi)\ , \tag{C1}$$

where the Y_n are spherical harmonics. Requiring that pressure and velocity be continuous at the surface of the bubble yields, to linear order in $a(t)$,

$$\ddot{a}_n+\frac{3\dot{R}}{R}\dot{a}_n-\left[(n-1)\frac{\ddot{R}}{R}\right]a_n=0\ . \tag{C2}$$

In the equation above surface tension and viscosity, which tend always to dampen the corrugations of the bubble surface have been neglected. To investigate the susceptibility of the bubble to corrugations, it is helpful to consider separately three regimes of the SL bubble motion. During the expansion of the bubble to R_m, the growth is quite accurately linear. The corresponding solution for $a(t)$ decreases as $1/R^2$ from its initial value. During the collapse from the maximum, the bubble obeys

$$\dot{R}^2=\frac{2}{3}\frac{P_0}{\rho_l}\left[\frac{R_m^3}{R^3}-1\right]\ , \tag{C3}$$

which is Rayleigh's solution for a collapsing vacuous cavity [8]. For this motion equation (C2) can be rewritten in the form [21,22]

$$y(1-y)a_n''(y)+\left[\frac{1}{3}-\frac{5}{6}y\right]a_n'(y)$$
$$-\frac{(n-1)}{6}a_n(y)=0\ , \tag{C4}$$

where $y\equiv R_m^3/R^3$. The asymptotic solution of this hypergeometric equation, as $y\to\infty$, is $a_n\sim(R_m/R)^{1/4}$. Since the Rayleigh expression (C3) is true to radii of the order R_0, before the gas pressure affects the collapse, the enhancement of the surface corrugation is only a factor of about $10^{1/4}\approx1.8$. Alternatively, (C2) can be written in a Hamiltonian form

$$H=\frac{p_n^2}{2R^3\rho_l}-\frac{(n-1)}{2}R^2\ddot{R}a_n^2\rho_l\ , \tag{C5}$$

where p_n is the momentum canonical to a_n. Since $\ddot{R}$ is negative during the collapse, the motion in the "potential well" of the Hamiltonian is stable, and the magnification of corrugations is due to the scaling of the effective mass and the potential through R in the spherical geometry. Following the collapse the bubble is virtually motionless at R_0 for one half of the acoustic cycle. Applying Eq. (C2) yields a linear growth of $a(t)$ during that time. Including corrections due to surface tension σ_l and viscosity η_l shows that the more accurate solution during that part of the motion where the bubble radius is constant is [22]

$$a_n(t)=a_0\cos(\omega_\sigma t+\delta_0)e^{-\alpha t}\ , \tag{C6}$$

where

$$\omega_\sigma^2=\frac{(n-1)(n+1)(n+2)\sigma_l}{R_0^3\rho_l}$$

and

$$\alpha=\frac{(n+2)(2n+1)\eta_l}{R_0^2\rho_l}\ .$$

In particular the time constant for a quadrupolar perturbation to decay for a bubble motionless at $R_0=4$ μm is less than 1 μsec. The instabilities associated with the collapse of the bubble to its minimum cannot be analyzed within this simplified framework, since even the hydrodynamics is violated at the minimum. We conclude that during any given cycle, i.e., from flash to flash, spherical modulations do not build up. The upper threshold of SL is due to either some other hydrodynamic instability or to an event occurring at the moment of collapse, which is not describable by hydrodynamics.

[1] C. A. Bjerknes, in *Fields of Force,* edited by V. F. J. Bjerknes (Columbia University Press, New York, 1906); K. Yosioka and Y. Kawasima, Acustica **5**, 167 (1955); R. Löfstedt and S. Putterman, J. Acoust. Soc. Am. **90**, 2027 (1991). [Additional work on radiation forces is found in: F. G. Blake, Jr., Tech. Memo 12, Acoust. Res. Lab., Harvard (1949); R. K. Gould, J. Acoust. Soc. Am. **56**, 1740 (1974); M. Strasberg, *ibid.* **33**, 359 (1961); L. A. Crum, *ibid.* **68**, 203 (1980).]

[2] M. M. Fyrillas and A. J. Szeri, J. Fluid Mech. **277**, 381 (1994).

[3] A. Eller and H. G. Flynn, J. Acoust. Soc. Am. **37**, 493 (1965). (There is much related work on the topic of "rectified diffusion" found in the parenthetic citations of Ref. [1].)

[4] B. P. Barber and S. J. Putterman, Nature **352**, 318 (1991); R. Hiller, S. J. Putterman, and B. P. Barber, Phys. Rev. Lett. **69**, 1182 (1992).

[5] B. Barber, R. Löfstedt, and S. Putterman, J. Acoust. Soc. Am. Suppl. 1 **89**, S1885 (1991).

[6] B. P. Barber *et al.*, Phys. Rev. Lett. **72**, 1380 (1994).

[7] R. Hiller *et al.*, Science **266**, 248 (1994).

[8] Lord Rayleigh, Philos. Mag. **34**, 94 (1917).

[9] M. Plesset, J. Appl. Mech. **16**, 277 (1949).

[10] R. Löfstedt, B. P. Barber, and S. J. Putterman, Phys. Fluids A **5**, 2911 (1993).

[11] A. Prosperetti, Rend. Sc. Int. Fis. "Enrico Fermi" **XCIII**, 145 (1984); A. Prosperetti, L. Crum, and K. Commander, J. Acoust. Soc. Am. **83**, 502 (1988).

[12] H. P. Greenspan and A. Nadim, Phys. Fluids A **5**, 1065 (1993); C. C. Wu and P. H. Roberts, Phys. Rev. Lett. **70**, 3424 (1993); W. C. Moss *et al.*, Phys. Fluids **6**, 2979 (1994).

[13] E. Fermi, *Thermodynamics* (Dover, New York, 1936), Sec. 28.

[14] S. J. Putterman *et al.* (patent application).

[15] R. Battino, T. Rettich, and T. Tominaga, J. Phys. Chem. Ref. Data **13**, 563 (1984).

[16] L. D. Landau and E. M. Lifshitz, *Fluid Mechanics,* 2nd ed. (Pergamon, New York, 1987), Sec. 59.

[17] L. D. Landau and E. M. Lifshitz, *Statistical Mechanics,* 3rd ed. (Pergamon, New York, 1980), Sec. 87.

[18] Ref. [16], Sec. 52.

[19] R. K. Gould, J. Acoust. Soc. Am. **56**, 1740 (1973); T. J. Asaki, P. L. Marston, and E. H. Trinh, *ibid.* **93**, 706 (1993).

[20] Lord Rayleigh, Proc. London Math. Soc. **XIV**, 170 (1883); G. I. Taylor, Proc. R. Soc. London Ser. A **201**, 192 (1950).

[21] M. S. Plesset and T. P. Mitchell, Quart. Appl. Math. **XIII**, 419 (1956).

[22] A. Prosperetti, Quart. Appl. Math. **34**, 339 (1977).

[23] P. S. Epstein and M. S. Plesset, J. Chem. Phys. **18**, 1505 (1950).

[24] B. P. Barber *et al.*, J. Acoust. Soc. Am. **91**, 3061 (1992).

[25] D. F. Gaitan and L. A. Crum, in *Frontiers of Nonlinear Acoustics,* Proceedings of the 12th International Symposium on Nonlinear Acoustics, edited by M. Hamilton and D. T. Blackstock (Elsevier, New York, 1990).

[26] D. F. Gaitan *et al.*, J. Acoust. Soc. Am. **91**, 3166 (1992); R. G. Holt *et al.*, Phys. Rev. Lett. **72**, 1376 (1994).

[27] B. P. Barber and S. J. Putterman, Phys. Rev. Lett. **69**, 3839 (1992).